Molecular Bottlebrushes†

Matthias Wintermantel, Markus Gerle, Karl Fischer, and Manfred Schmidt*

Universität Bayreuth, Makromolekulare Chemie II, D-95440 Bayreuth, Germany

Isao Wataoka, Hiroshi Urakawa, Kanji Kajiwara, and Yasuhisa Tsukahara

Kyoto Institute of Technology, Kyoto 606, Japan

Received February 22, 1995; Revised Manuscript Received September 25, 1995[⊗]

ABSTRACT: Polymacromonomers consisting of oligostyrene side chains ($700 \leq M_n \leq 5000$ g/mol) and of a high molar mass polymethacrylate main chain are shown to exhibit a bottlebrush structure in that the PMA main chain adopts an extremely stiff conformation (i.e., a Kuhn statistical segment length of up to $l_k = 2000$ Å) which is surrounded by the expanded but still flexible polystyrene side chains.

Introduction

In a previous communication, we reported on the conformation of one polymacromonomer with a side chain length of 28 styrene units.[1] Neglecting the effect of butyl groups originating from the initiator and of the ethylene oxide/methacryloyl moieties on the refractive index increment of the polymer, i.e., assuming $dn/dc = 0.108$ cm^3/g for polystyrene, the radius of gyration vs the molar mass relationship could well be fitted by a wormlike chain model of $l_k = 1000$ Å, if the contour length per monomer is taken as $l = 2.5$ Å (all-trans conformation). Qualitatively similar conclusions were drawn from diffusion and sedimentation measurements,[2] whereas viscosity results are not well understood.[1,3]

In the present publication, we additionally reanalyze the former data in terms of exact refractive index increments (i.e., polymacromonomer molar mass) and exact macromonomer molar mass obtained by mass spectrometry and provide measurements on polymers with different side chain lengths. The cross-sectional characteristics of such "molecular bottlebrushes" are investigated by X-ray scattering (cross-sectional radius of gyration, $R_{g,c}$) and by the hydrodynamically effective diameter, d_h, as derived from the diffusion coefficient measured by dynamic light scattering.

Experimental Section

The synthesis of methacryloyl end-functionalized polystyrene macromonomers by anionic polymerization and the subsequent radical homopolymerization of the macromonomer was performed as described elsewhere.[4−6] Two sets of samples were investigated which were prepared in Kyoto (samples KPS*X*MA*Y* with *X* the approximate macromonomer molar mass and *Y* the approximate degree of polymerization of the polymacromonomer main chain) and in Bayreuth (samples BPS*X*MA*Y*), respectively. The light scattering characterization of the polymacromonomers is summarized in Table 1.

The macromonomer molar mass, M_n, was determined by a MALDI-TOF spectrometer (Bruker, reflection mode) utilizing a 5-chlorosalicylic acid matrix which contained silver ions in form of $AgCF_3COO$. Since no unreacted macromonomer was available for the Kyoto samples, part of the polymers were hydrolyzed and the resulting oligostyrenes, each with an ethanolic end group, were analyzed. The characterization of the macromonomers is shown in Table 2. A detailed comparison of the MALDI-TOF results with size exclusion and adsorption chromatography will be presented elsewhere.[8]

Table 1. Light Scattering Characterization of Polymacromonomers with Different Side Chain Length[a]

sample	dn/dc (cm^3 g^{-1})	$M_w \times 10^{-6}$ (g mol^{-1})	R_g (nm)	R_h (nm)	R_g/R_h
KPS800MA258	0.081	0.2	15.0		
KPS800MA549		0.496	25.5		
KPS800MA1730		1.5	43.0		
BPS1000MA903	0.0896	0.894	25.7	17.6	1.46
BPS1700MA1867	0.0914	3.1	47.7	30.0	1.59
KPS2900MA165	0.096	0.577	16.0	11.0	1.45
KPS2900MA212		0.872	19.0	13.4	1.42
KPS2900MA1019		3.17	51.0	24.5	2.08
BPS3900MA558	0.1031	2.2	41.6	27.4	1.52
BPS4000MA602	0.1031	2.38	40.0	25.0	1.6
BPS5000MA547	0.1046	2.70	44.7	22.4	2.0
KPS5500MA59		0.342	11.0	10.5	1.05
KPS5500MA216	0.1060	1.27	23.5	17.7	1.32
KPS5500MA305		1.91	28.0	21.0	1.33

[a] The routine measurements exhibit errors of approximately ±1% of dn/dc, ±2% for R_h, and ±3% for M_w and R_g.

Table 2. Characterization of the Macromonomers by Mass Spectroscopy (MALDI-TOF-MS)

sample	M_n (g mol^{-1})	M_w (g mol^{-1})	M_w/M_n
KPS800MA1	720	770	1.07
BPS1000MA1	990	1030	1.04
BPS1700MA1	1660	1740	1.04
KPS2900MA1	2780	2870	1.03
BPS3900MA1	3940	4000	1.015
BPS4000MA1	3950	4040	1.024
BPS5000MA1	4940	5050	1.021
KPS5500MA1	4940	5180	1.048

Small-angle X-ray scattering experiments were carried out with the small-angle equipment for solutions[9] installed on the 2.5 GeV storage ring in the Photon Factory, KEK, Tsukuba, Japan. The intensities of all samples including solvent were measured at 25 °C with a wavelength of $\lambda_0 = 0.149$ nm for a 600 s duration at 512 different scattering angles. Manipulation of the data and the detailed experimental procedure are described elsewhere.[10]

Dynamic light scattering measurements were performed with standard equipment utilizing an ALV SP-86 goniometer and either an ALV 3000 correlator and a Kr ion laser light source (647.1 nm wavelength, 500 mW power) or an ALV 5000 correlator and a Nd-YAG laser (532.0 nm, 80 mW power). Correlation functions were analyzed by the method of cumulants.

† Dedicated to Prof. Werner Borchard on the occasion of his 60th birthday.

⊗ Abstract published in *Advance ACS Abstracts,* December 15, 1995.

0024-9297/96/2229-0978$12.00/0

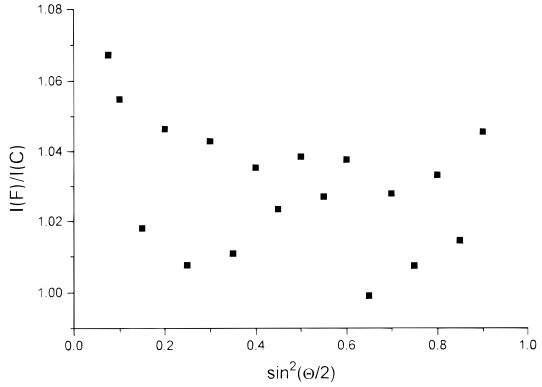

Figure 1. Increased scattering intensity of toluene in the flow cell (I_f) as compared to toluene in a 20 mm cuvette (I_c) for the different scattering angles, expressed as $\sin^2(\theta/2)$.

The structure characterization of the polymacromonomers was performed with a size exclusion chromatography connected to an on-line Knauer combined viscometer/refractive index detector and an ALV 1800 multiangle light scattering instrument equipped with an Ar ion laser operating at 514 nm (300 mW power) and with a home-made, cylindrical flow cell with a 38 μL total volume.[1,11] The size exclusion chromatography (SEC) was performed in toluene on polystyrene gel columns (5 μm, 10^4 Å, 10^5 Å, 10^6 Å nominal pore diameter, PSS Co., Mainz). Typical runs utilized a 100 μL injection volume and a 2−3 g/L polymacromonomer concentration.

The absolute calibration of the light scattering detection system was performed by toluene in a "state of the art" cylindrical Suprasil cuvette with a diameter of 20 mm which was subsequently replaced by a cylindrical flow cell, also consisting of schlieren-free Suprasil, with a 6 mm inner diameter, a 20 mm outer diameter, and a 1 mm height. The scattering intensity of the flowing toluene was then recorded as solvent scattering, which was later subtracted from the scattering intensity measured from the eluting macromolecules in order to determine the "excess" scattering intensity. It should be noted that the scattering intensities of toluene in the flow cell were always slightly higher as compared to the 20 mm cuvette, because some extraneous scattering, particularly at small and large scattering angles, caused by reflections in the flow cell was unavoidable and could only be minimized. A typical pattern is shown in Figure 1, where the ratio of the scattering intensities of the flow cell and the 20 mm cell is shown for the different scattering angles. This ratio is expected to increase with increasing refractive index difference between solvent and Suprasil ($n_D = 1.479$) but has not yet been quantified for solvents other than toluene for our flow cell design. Careful inspection of Figure 1 reveals the scattering intensity to exhibit an oscillatory pattern in alternate scattering angles. This originates from the fact that the scattering angles are distributed on both sides of the cuvette, i.e., in a 360° circle with alternate angles on different sides. The pattern simply reflects the accidental fact that extraneous light is a bit higher on the right-hand side of the cuvette as compared to the left-hand side. Within a few percent, such subtle effects are definitely beyond the control of the operator.

One important point is that the scattering pattern shown in Figure 1 does not alter with time, if the flow cell position remains unchanged, but the pattern does change when reinserting the flow cell into the light scattering instrument. Keeping the cell position constant ensures that all extraneous light is subtracted via the solvent scattering and that the calibration of the instrument by the 20 mm cuvette is precise within ±0.2% for all scattering angles (±0.1% for repeated measurements of 1 s duration with the cell position unchanged). The details described above are absolutely crucial for precise and correct measurements of the molar mass and radius of gyration, because for calibration purposes the influence of extraneous light has to be completely eliminated. Moving the cell after solvent recording could seriously influence the measurement range at small excess scattering

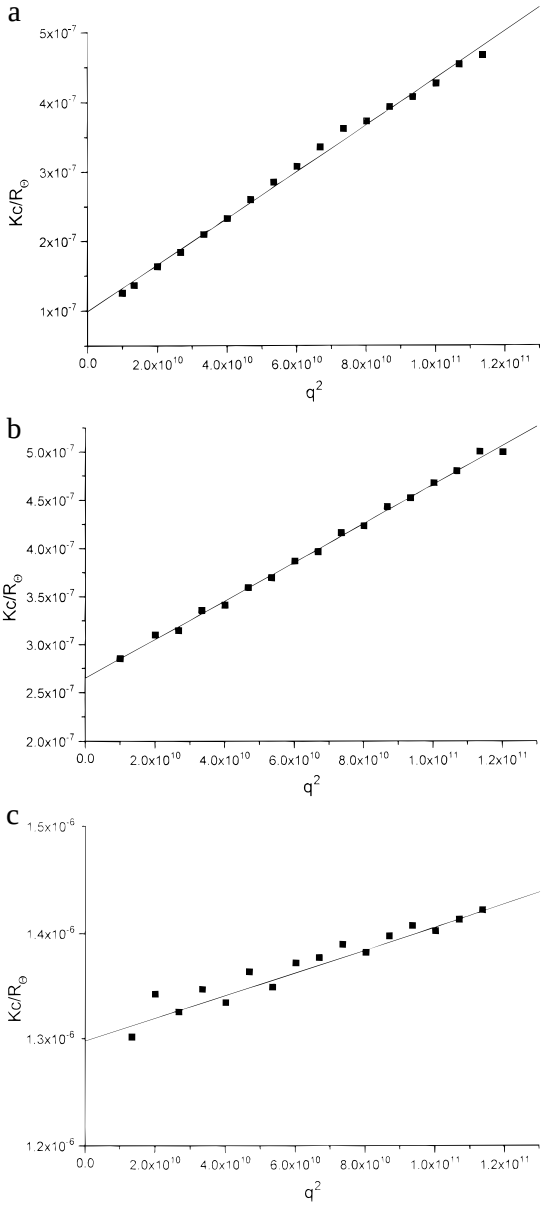

Figure 2. Online measured reduced scattering intensity Kc/R_θ vs q^2 for polymacromonomer BPS4000MA obtained at different elution times: (a) $c = 6.22 \times 10^{-3}$ g/L ($M_w = 1.01 \times 10^7$ g/mol, $R_g = 100.6$ nm); (b) $c = 4.21 \times 10^{-2}$ g/L ($M_w = 3.77 \times 10^6$ g/mol, $R_g = 47.7$ nm); (c) $c = 4.14 \times 10^{-2}$ g/L ($M_w = 7.61 \times 10^5$ g/mol, $R_g = 14.3$ nm).

intensities and could also cause systematic errors if the changes of the scattering pattern are not random. Typically, the scattering intensity is averaged over a period of 2 s and subsequent measurements during the elution of the sample are taken every 4 s. In order to document the quality of the measurements, the angular dependence of the reduced scattering intensity is shown during the elution of the polymacromonomer BPS4000MA602 in Figure 2a−c.

Despite the extremely low concentrations of $c = 6.22 \times 10^{-3}$ g/L, the eluting high molar mass fractions are measured with high accuracy (Figure 2a) which even increases toward the light scattering peak concentrations $c = 4.21 \times 10^{-2}$ g/L (Figure 2b). Only at the small molar mass regime do the data scatter significantly, but still allow a reasonably accurate determination of the radius of gyration (Figure 2c, $c = 4.14 \times 10^{-2}$ g/L). In general, the uncertainties in the extrapolations as shown above are much smaller than the symbol size in the following Figures 3−5 and never exceed the size of symbols even at the very low concentrations in both wings of the distribution. The reproducibility can be estimated by the overlap of different molar mass samples as shown in Figures 3−5.

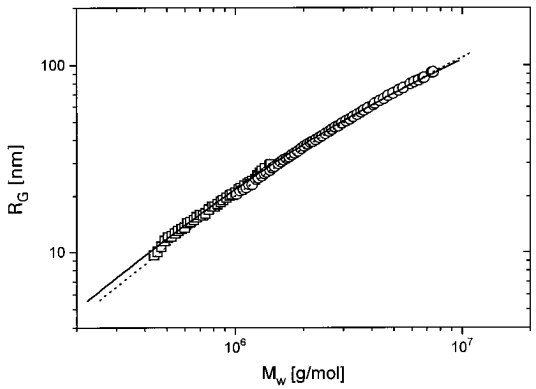

Figure 3. Radius of gyration−molar mass relation for polymacromonomers KPS2900MA165 (◇) and KPS2900MA1019 (○). Solid line: wormlike chain theory with l_k = 890 Å and l = 2.5 Å. Dotted line: l_k = 1130 Å, l = 2.2 Å.

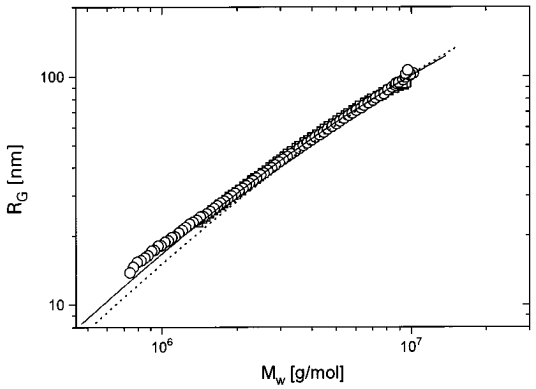

Figure 4. Radius of gyration−molar mass relation for polymacromonomers BPS3900MA558 (◇) and BPS4000MA602 (○). Solid line: l_k = 1280 Å, l = 2.5 Å. Dotted line: l_k = 1690 Å, l = 2.2 Å.

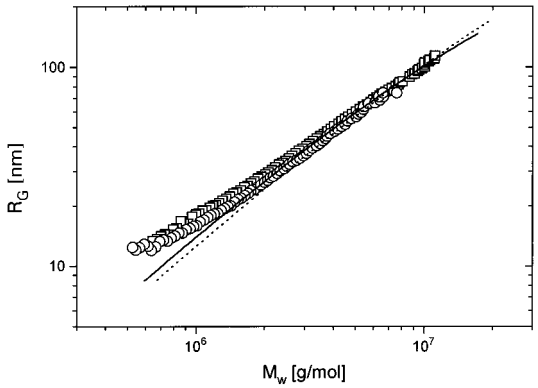

Figure 5. Radius of gyration−molar mass relation for polymacromonomers BPS5000MA547 (◇) and KPS5500MA305 (○). Solid line: l_k = 2076 Å, l = 2.5 Å. Dotted line: l_k = 3329 Å, l = 2.2 Å.

Results and Discussion

In Figures 3−5, the measured R_g−M relations of some polymacromonomers are shown for different side chain molar masses where the lines represent the best fit of the data by a wormlike chain model, i.e.

$$R_g^2 = \frac{L l_k}{6} - \frac{l_k^2}{4} + \frac{l_k^3}{4L} - \frac{l_k^4}{8L^2}(1 - \exp(-2L/l_k)) \quad (1)$$

with L the contour length of the chain and l_k the Kuhn statistical segment length.

A fit of the data according to eq 1 requires precise knowledge of the contour length L, which is usually derived from the molar mass and the known length of a monomer unit, l, i.e., 2.5 Å for a vinyl main chain. It should be noted, however, that in principle l could be considerably smaller if some degree of stereoregularity forces the main chain into a helical conformation. Whereas for usual radical polymerizations this effect is negligible, a stereospecific addition of the monomers could result for the present highly overcrowded structures. In Figures 3−5 the best fits of the Kuhn statistical segment length are shown for l = 2.5 Å (full curves) and—arbitrarily chosen—for l = 2.2 Å (dotted curves). The qualities of both fits are excellent and do not allow an unambiguous choice of l. As deduced from the l_k values listed in Table 3, l_k values derived by l = 2.5 Å are always smaller than those fitted with l = 2.2 Å. The former represent the lower limit of the experimentally determined chain stiffness, because l > 2.5 Å values would lead to unphysical bond angles. Restricting the discussion to the l = 2. 5 Å results, the chain stiffness is found to increase with the side chain molar mass M_{sc} for l_k = 890 Å for M_{sc} = 2780 g/mol to l_k = 1280 Å for M_{sc} = 3950 g/mol to l_k = 2076 Å for M_{sc} = 4940 g/mol. The coincidence in the side chain molar masses of the samples prepared in Kyoto and Bayreuth as shown in Figure 5 is accidental, and fortunately no difference between the samples prepared at the different locations is observed.

With increasing side chain length, the theoretical curve utilizing the wormlike chain model deviates from the data in the small molar mass regime. This is most probably caused by the onsetting influence of the finite cross-section of the chains when the main chain degree of polymerization becomes only slightly larger than that of the side chain.

The polymacromonomers with side chain molar masses M_n < 2000 g/mol yield R_g−M relations which cannot be well fitted by the wormlike chain model as shown for the samples BPS1000MA903 and BPS1700MA1867 in Figure 6. It should be noted that the smaller side chain curve lies above the larger side chain curve because of the significantly smaller contour length at the same polymer molar mass which is not completely compensated by the increased chain stiffness. Although the Kuhn length is approximately given by $l_k \cong$ 230 Å and by $l_k \cong$ 390 Å, respectively, the theoretical lines deviate significantly from the measured data. One explanation for this discrepancy could originate from the molar mass distribution of the macromonomer. Parts a and b of Figure 7 show the MALDI-TOF results and the HPLC trace, respectively, for the BPS1000MA1 sample. It is seen that the sample is composed of tetramers up to pentadecamers, with a maximum occurrence of octamers. The numbers attached to the peaks in Figure 7 refer to the number of styrene units in the macromonomer. The molar masses shown at the top of Figure 7a, e.g., 1111.8 g/mol, have to be reduced by the molar mass of silver (108), by the butyl group from the initiator (57), and by the ethoxymethacrylate (113) in order to arrive at M = 833.8 g/mol, which is in good agreement with M = 833.2 g/mol for the polystyrene octamer; the small difference is caused by calibration inaccuracies. Nonetheless, the point to be stressed here is that both MALDI-TOF and HPLC identify exactly the same number of peaks.

Since the rate of polymerization of tetramers and pentamers is much larger than that for decamers and higher molar mass macromonomers, a heterogeneous sample could result, as predominantly more flexible

Table 3. Kuhn Statistical Segment Length l_k, Twice the Contour Length of the Side Chain $2L_s$, the Hydrodynamically Effective Diameter of the Cylinder d_h, the Measured Cross-Sectional Radius of Gyration $R_{g,c}$, and the Effective "Hard-Core" Diameter d_{eff} for Different Polymacromonomers[a]

sample	Kuhn length l_k (Å) with l = 2.5 Å	Kuhn length l_k (Å) with l = 2.2 Å	d_h (Å)	$R_{g,c}$ (Å)	d_{eff} (Å)
KPS800MA1730	(261)	(300)		12.2	34.5
BPS1000MA903	(232)	(273)	60[c]		
BPS1700MA1867	(390)	(454)	80[c]		
KPS2900MA*Y*[b]	890	1130	80	31.5	89.1
BPS3900MA*Y*[b]	1280	1690	150	36.4	103.0
BPS4000MA602	1280	1690	100[c]		
BPS5000MA547	2076	3329	100[c]		
KPS5500MA*Y*[b]	2076	3329	180	52.0	147.1

[a] The numbers in parentheses represent approximate "mean" values; see text. [b] Y indicates that the results are derived from several samples with different main chain lengths. [c] Approximate values derived from a single data fit only.

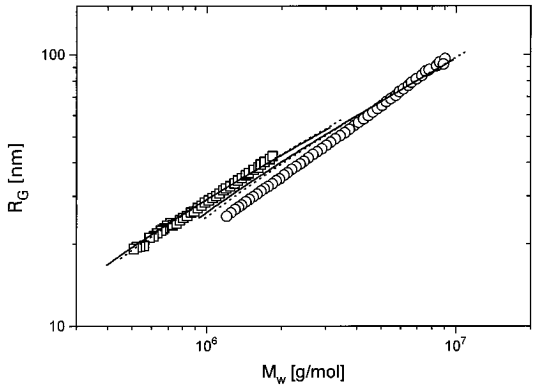

Figure 6. Radius of gyration−molar mass relation for polymacromonomers BPS1700MA1867 (○) and BPS1000MA903 (◇). Solid lines: l_k = 390 Å and l_k = 232 Å, l = 2.5 Å. Dotted lines: l_k = 454 Å and l_k = 273 Å, l = 2.2 Å.

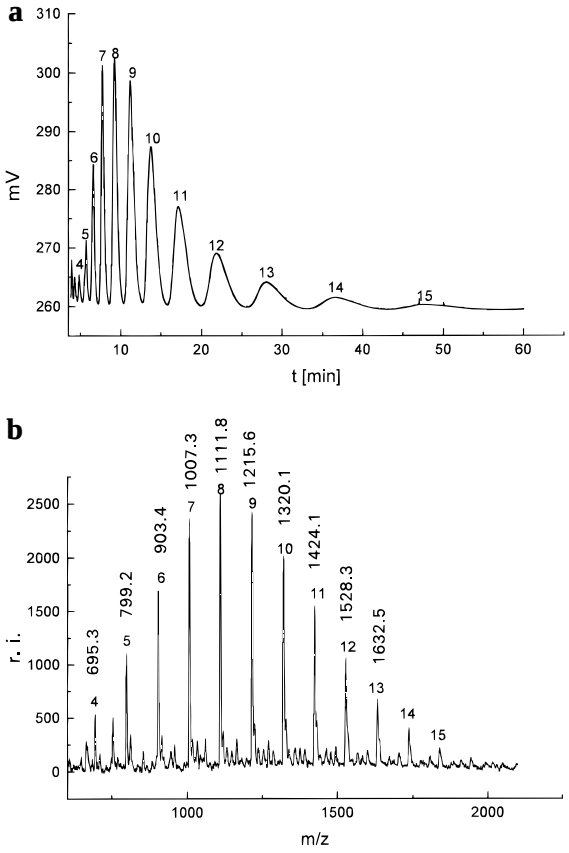

Figure 7. MALDI-TOF mass spectrum (a) and HPLC trace (b) of the macromonomer BPS1000MA1.

small side chain polymacromonomers are formed at the beginning and stiffer large side chain polymers are formed toward the end of the polymerization. This

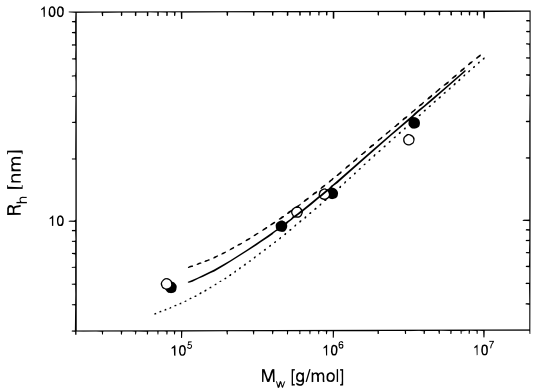

Figure 8. Hydrodynamic radius—molar mass relation for polymacromonomer KPS2900MA*Y*: (●) fractionated; (○) unfractionated. Solid line: l_k = 890 Å, d_h = 60 Å. Dashed line: l_k = 890 Å, d_h = 100 Å.

would result in a mixture of more and less flexible polymers eluting at the same time which cannot be fitted theoretically. Also, due to the "quasi-living" character of the polymerization, a block copolymer character of the polymers could result with one end more flexible than the other. Only for larger side chain macromonomers of $M_n \geq$ 2000 g/mol does the reactivity difference become negligible between the homologues and, additionally, the chain stiffness no longer critically depends on the side chain length. This point will be addressed in a future work where, for instance, the pentamer will be isolated and polymerized.

The origin of the stiffness of the main chain is not yet clear. Possible explanations are (i) simple steric overcrowding, (ii) specific phenyl ring interaction, i.e., stacking, and (iii) a certain degree of tacticity caused by the steric requirements during the addition of a monomer to the highly overcrowded radical at the chain end. The different possibilities will be investigated in a future work on polymacromonomers without phenyl rings in the side chain and by NMR investigations of ^{13}C labeled methacryloyl groups in the main chain.

In order to support the conclusion drawn from the R_g−M measurements, dynamic light scattering was performed on narrow fractions of the eluting polymers, as previously described, the results of which are shown in Figures 8 and 9 for the samples KPS2900MA*Y* and BPS3900MA*Y* in terms of the hydrodynamic radius R_h which is derived from the measured diffusion coefficient via Stoke's law

$$R_h = \frac{KT}{6\pi\eta_0 D} \tag{2}$$

with KT the thermal energy and η_0 the solvent viscosity.

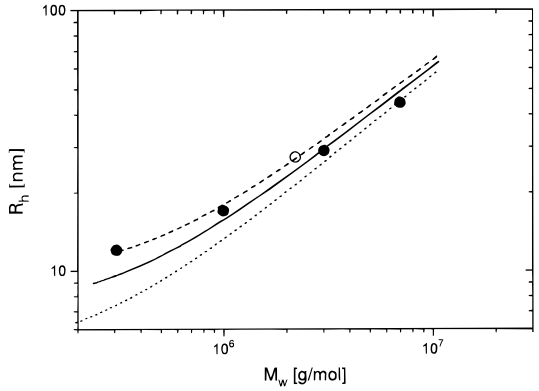

Figure 9. Hydrodynamic radius−molar mass relation for polymacromonomer BPS3900MA*Y*: (●) fractionated; (○) unfractionated. Solid line: wormlike chain theory with $l_k = 1280$ Å, $d_h = 150$ Å. Dotted line: $l_k = 1280$ Å, $d_h = 100$ Å. Dashed line: $l_k = 1280$ Å, $d_h = 200$ Å.

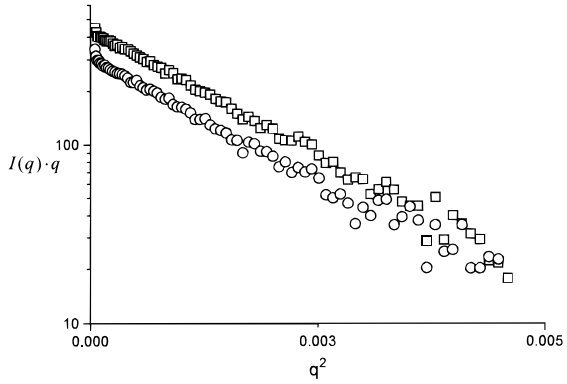

Figure 10. X-ray scattering on polymacromonomer BPS-3900MA558 at two different concentrations: (□) $c = 2.66$ g/L; (○) $c = 3.42$ g/L. Ignoring the upturn at small q, the linear slope at high q values yields the cross-sectional radius of gyration, $R_{g,c} = 36.4$ Å.

Unfortunately, the hydrodynamic radius of stiff polymers depends not only on the contour length L and on the Kuhn length l_k but also on the hydrodynamically effective cross section, d_h, of the chain.[12] Thus, the hydrodynamic data alone will not allow the determination of chain stiffness without knowledge of d_h and vice versa. We here keep L (with $l = 2.5$ Å) and l_k fixed as derived from the analysis of the R_g-M plot and determine d_h from the best fit to the data.

The results are shown in Figures 8 and 9 and the corresponding d_h values are given in Table 3. The fact that good fits with reasonable d_h values can be achieved merely indicates that also the diffusion data are compatible with the interpretation in terms of a large chain stiffness. It should be noted that for given L and l_k, $R_h \sim 1/\ln(L/d_h)$; i.e., small errors in R_h result in a large uncertainty in the d_h values, which is reflected in the scatter of the d_h values shown in Table 3.

In order to obtain more information concerning the side chain dimensions, the cross-sectional radius of gyration was determined by X-ray scattering from the slope of $\ln(I(q)q)$ vs q^2 as shown for sample BPS3900MA in Figure 10 (see also Table 3). Also here, the side chain conformation is only qualitatively characterized because there is no definite relation between the single side chain radius of gyration and the measured cross-sectional one, except for cylinders of uniform or well-defined segment density. In a future work, this question will be addressed quantitatively by using copolymers with deuterated and hydrogenated side chains.

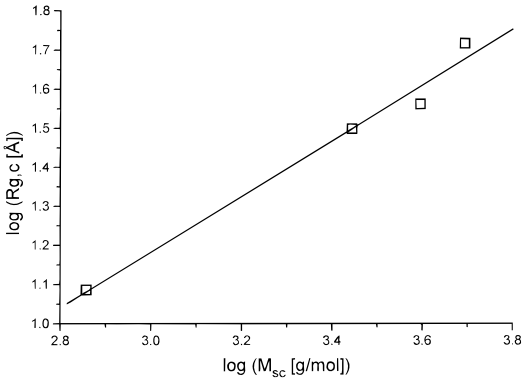

Figure 11. Double-logarithmic plot of the cross-sectional radius of gyration vs the side chain molar mass. The least squares fit to the values is shown by the solid line with a 0.71 slope.

Presently, we assume a constant segment density across the cylinder and derive an effective diameter

$$d_{eff} = \sqrt{8} R_{g,c} \tag{3}$$

from the measured $R_{g,c}$ which is included in Table 3.

So far, we have no evidence on the expansion of the side chains due to overcrowding. However, scaling arguments predict the layer thickness d_l to scale with the side chain length or side chain molar mass as[13]

$$d_l \sim M_{sc}^{3/4} \tag{4}$$

for flexible chains tethered to a straight line (cylinders). An experimental test of eq 4 is shown in Figure 11, where the layer thickness d_l is identified with the measured cross-sectional radius of gyration. Although only four data points are available, the experimentally determined exponent of 0.71 seems to support the scaling relation eq 4. Still, the results should be taken with caution because the assumed proportionality between d_l and $R_{g,c}$ holds only if the segment density profile perpendicular to the long cylinder axis does not change with the side chain molar mass. To the best of our knowledge this is the first experimental evidence for scaling arguments of flexible chains attached to a cylindrical surface.

As already reported in a previous publication,[1] the viscosity−molar mass relations do not support the conclusion derived from the light scattering experiments. It was previously speculated that the difference is due to the failure of the wormlike chain theory when applied to such "bottlebrush"-like structures, which exhibit no "hard-core" cross-sectional density profile but rather a decaying segment density toward the cylindrical surface. We here confine our discussion to the statement that the present data (not shown) support this hypothesis as the deviation from the wormlike chain theory increases with increasing side chain lengths in exactly the same manner as shown in Figure 3 to ref 1. Certainly, much more theoretical effort is needed in order to derive a viscosity theory for such complex structures.

Conclusion

Multidetection GPC consisting of a multiangle light scattering and a viscosity detector constitutes an extremely powerful technique for the structure determination of complex molecular architectures. Applied to the characterization of polymacromonomers, the exceed-

ingly high main chain stiffness of such "overcrowded" structures is unambiguously proven, thus establishing an easy route to prepare rodlike macromolecules consisting of "commodity" monomers. Such structures are expected to form lyotropic main chain liquid crystals, which have indeed been observed.[14,15]

Acknowledgment. Financial support of the Deutsche Forschungsgemeinschaft and the Fonds der Chemischen Industrie is gratefully acknowledged.

References and Notes

(1) Wintermantel, M.; Schmidt, M.; Tsukahara, Y.; Kajiwara, K.; Kohjiya, S. *Macromol. Rapid Commun.* **1994**, *15*, 279.
(2) Nemoto, N.; Nagai, M.; Koike, A.; Okada, S., in preparation.
(3) Tsukahara, Y.; Kohjiya, S.; Tsutsumi, K.; Okamoto, Y. *Macromolecules* **1994**, *27*, 1662.
(4) Tsukahara, Y.; Mizuno, K.; Segawa, A.; Yamashita, Y. *Macromolecules* **1989**, *22*, 1546.
(5) Tsukahara, Y.; Tsutsumi, K.; Yamashita, Y.; Shimada, S. *Macromolecules* **1990**, *23*, 5201.
(6) Tsukahara, Y. In *Macromolecular Design: Concept and Practice*; Mishra, M., Ed.; Polymer Frontiers International Inc.: New York, 1994; pp 161−227.
(7) We here utilize the approximate molar mass X in order to allow identification of the samples in former publications of Tsukahara et al. The side chain molar mass, M_{sc}, introduced later represents the exact value.
(8) Spickermann, J.; Räder, J.; Müllen, K.; Gerle, M.; Schmidt, M., in preparation.
(9) Ueki, T.; Hiragi, Y.; Izumi, Y.; Tagawa, H.; Kataoka, M.; Muroga, Y.; Matsushita, T.; Amemiya, Y. *Photon Factory Activity Report* **1983**, *82/83*, 70.
(10) Hiragi, Y.; Inoue, H.; Sano, Y.; Kajiwara, K.; Ueki, T.; Kataoka, M.; Tagawa, H.; Izumi, Y.; Muroga, Y.; Amemija, Y. *J. Mol. Biol.* **1988**, *204*, 129.
(11) Wintermantel, M.; Antonietti, M.; Schmidt, M. *J. Appl. Polym. Sci., Polym. Symp.* **1993**, *52*, 91.
(12) Yamakawa, H.; Fujii, M. *Macromolecules* **1974**, *7*, 128.
(13) Halperin, A.; Tirrell, M.; Lodge, T. P. *Adv. Polym. Sci.* **1992**, *100*, 31.
(14) Wintermantel, M.; Fischer, K.; Gerle, M.; Ries, R.; Schmidt, M.; Kajiwara, K.; Urakawa, H.; Wataoka, I. *Angew. Chem.* **1995**, *107*, 1606.
(15) Tsukahara, Y.; Ohta, Y.; Senoo, K. *Polymer* **1995**, *36*, 3413.

MA950227S